IVYSPRING INTERNATIONAL PUBLISHER

Theranostics

2016; 6(8): 1105-1118. doi: 10.7150/thno.14700

Research Paper

MiR675-5p Acts on HIF-1α to Sustain Hypoxic Responses: A New Therapeutic Strategy for Glioma

Alessia Lo Dico[1,9*], Viviana Costa[2*], Cristina Martelli[3], Cecilia Diceglie[3,4], Francesca Rajata[5], Aroldo Rizzo[5], Carmine Mancone[6], Marco Tripodi[6,7], Luisa Ottobrini[3,8], Riccardo Alessandro[9,10#✉], Alice Conigliaro[6#✉]

1. Tecnomed Foundation of the University of Milano-Bicocca, Monza 20900, Italy
2. Laboratory of Tissue Engineering - Innovative Technology Platforms for Tissue Engineering (PON01-00829), Rizzoli Orthopedic Institute, Palermo 90127, Italy
3. Department of Pathophysiology and Transplantation, University of Milan, Milan 20100, Italy;
4. Doctorate School of Molecular Medicine, University of Milan, Milan 20100, Italy;
5. Unità Operativa di Anatomia Patologica, Azienda Ospedaliera Ospedali Riuniti "Villa Sofia-Cervello", Palermo 90100, Italy;
6. Dipartimento di Biotecnologie Cellulari ed Ematologia, Sapienza University of Rome, Rome 00185, Italy;
7. National Institute for Infectious Diseases L. Spallanzani, IRCCS, Rome 00149, Italy;
8. Institute of Molecular Bioimaging and Physiology (IBFM), National Researches Council (CNR), Segrate (MI) 20093, Italy;
9. Dipartimento di Biopatologia e Biotecnologie Mediche, University of Palermo, Palermo 90127, Italy;
10. Institute of Biomedicine and Molecular Immunology (IBIM), National Research Council of Italy, Palermo 90146, Italy.

* these authors contributed equally to this work.

joint senior authors.

✉ Corresponding authors: Alice Conigliaro (conigliaro@bce.uniroma1.it); Riccardo Alessandro (riccardo.alessandro@unipa.it).

Received: 2015.12.15; Accepted: 2016.04.14; Published: 2016.05.08

Abstract

Hypoxia is a common feature in solid tumours. In glioma, it is considered the major driving force for tumour angiogenesis and correlates with enhanced resistance to conventional therapies, increased invasiveness and a poor prognosis for patients. Here we describe, for the first time, that miR675-5p, embedded in hypoxia-induced long non-coding RNA H19, plays a mandatory role in establishing a hypoxic response and in promoting hypoxia-mediated angiogenesis. We demonstrated, *in vitro* and *in vivo*, that miR675-5p over expression in normoxia is sufficient to induce a hypoxic moreover, miR675-5p depletion in low oxygen conditions, drastically abolishes hypoxic responses including angiogenesis. In addition, our data indicate an interaction of miR675-5p, HIF-1α mRNA and the RNA Binding Protein HuR in hypoxia-induced responses. We suggest the modulation of miR675-5p as a new therapeutic option to promote or abolish hypoxia induced angiogenesis.

Key words: Angiogenesis, hypoxia, glioma, miRNA675, optical imaging, HuR, VHL.

Introduction

Hypoxia is a common feature in solid tumours and plays a key role in many aspects of tumour growth and development as well as in therapeutic response. Phenotypic changes, fundamental to malignant progression, are mediated by cellular hypoxia that, through the activation of several molecular cascades, induces genomic instability, loss of apoptotic potential, angiogenesis, resulting in an increase of metastasis and, finally, radio- or chemo-therapy resistance [1]. During malignant progression, the formation of hypoxic areas, within the expanding mass of a solid tumour, induces the so-called angiogenic switch, characterized by the stimulation of vessel growth [2, 3].

In glioma, hypoxia is considered the major driving force for tumour angiogenesis [4] and the Hypoxia Inducible Factor (HIF-1α) is the critical player in the establishment of vascular supply [5]. In normoxic conditions, HIF-1α is hydroxylated on proline residues (Pro402 and Pro564) by soluble Prolyl Hydroxylases (PHD), and targeted for rapid proteasomal degradation by the von Hippel-Lindau (VHL) tumour suppressor, the substrate recognition component of an E3-ubiquitin ligase. Loss of pVHL

function results in HIF-1α stabilization, increase of its transcriptional activity and subsequent up-regulation of HIF-1α target genes [6]. During hypoxia, prolyl-hydroxylation is prevented, thus allowing HIF-1α to escape proteolysis, dimerize with HIF-1β, and translocate to the nucleus where, it can directly promote neo-angiogenesis by inducing the expression of Vascular Endothelial Growth Factor (VEGF) [7, 8], the most powerful pro-angiogenic cytokine. Like VEGF, HIF-1α is able to activate a multitude of downstream genes involved in survival and proliferation (IGF-2, TGF-α, NOTCH-1), invasiveness (CXCR-4, MMP), new vessels formation (VEGF-A, VEGF-R1, ANGPT-1), metabolic adaptation (GLUT1/3, GAPDH) and pharmacological resistance [9] by binding Hypoxia Responsive Elements (HRE) in their enhancer and promoter regions [10].

Among the genes that were found to be altered in hypoxia in response to HIF-1α up-regulation, the long non-coding RNA (lncRNA) H19 was over-expressed in several tumours. H19 is considered as an oncogenic lncRNA, positively correlated with breast cancer [11, 12], bladder cancer [13, 14] and cervical carcinomas [15]. Ectopic H19 expression is able to enhance the tumorigenic potential of hepatocellular carcinoma cells *in vitro* and in animal models [16] and, as we recently described, it can also act as angiogenic inducer [17]. *H19* exon1 encodes for two conserved microRNAs, miR675-3p and miR675-5p, and it has been speculated that H19/miR-675 signalling axis plays an important role in carcinogenesis [18]. Recent studies have shown that miR675-5p expression is up-regulated in several cancer types such as glioma [19], gastric cancer [20, 21], colorectal cancer [18], skeletal muscle tumours and hepatocellular cancer [22]. However, a low expression of miR675-5p has been found in adrenal cortical carcinoma and metastatic prostate cancer cells [23, 24], implying that miR675-5p may play different roles depending on the tumour type. To our knowledge, no data have been reported up to date about the role of H19's miRNAs during hypoxia.

Here, we reveal a fundamental role of hypoxia-induced H19 and specifically of the H19-embedded miR675-5p that is required to sustain hypoxic responses, driving glioma angiogenesis and affecting endothelium. We demonstrated that the down-regulation of miR675-5p, in low O_2 partial pressure conditions, inhibits the hypoxic response by decreasing the nuclear HIF-1α and its mRNA. Moreover, our data indicate an involvement of the RNA binding protein HuR, which if bound to HIF-1α and VEGF mRNAs under hypoxic condition, was deregulated after miR675-5p depletion. In addition, miR-675-5p over expression in normoxia is able, *per se*, to promote hypoxic responses by driving HIF-1α nuclear accumulation and reducing VHL gene expression.

Finally, by combining *in vivo* administration of either the miR675-5p mimic or miR675-5p inhibitor and optical molecular imaging techniques in a preclinical glioma model, we identified miRNA675-5p as a new therapeutic target for glioma treatment.

Results

Validation of suitable cellular models for hypoxia studies

In order to preliminarily investigate the effects of hypoxia *in vitro* on critical cytotypes involved in glioblastoma progression, we used two widely accepted cellular models: the glioblastoma cell line U251 and Human Umbilical Vein Endothelial cells (HUVECs). The hypoxia responsiveness of both cell types was tested after incubation for six hours in a hypoxic chamber with 1% O_2 atmosphere. ELISA (**figure 1A)** and immunocytochemistry (**figure S1)** results show that both glioblastoma and endothelial cells respond to hypoxia by increasing HIF-1α nuclear levels. To functionally assess HIF-1α activity, the transcription of its target genes, involved in angiogenesis and metabolic changes, has been assessed by Real time-PCR analysis. As shown in **figure 1B**, HIF-1α up-regulation correlates with increased mRNA levels of its target genes involved in *i)* metabolic switch (GAPDH), *ii)* angiogenesis (VEGF) and *iii)* invasion and metastasis (CXCR-4, SNAIL, SLUG) whereas, other hypoxia-related genes (i.e. CAV-1 and Integrin-1), were not modulated. In addition, levels of soluble VEGF, the main driver of angiogenesis, were analysed by ELISA (**figure 1C**). Both cell lines increased VEGF secretion under hypoxia conditions, thus confirming that our cellular models respond to low oxygen conditions and therefore provide a suitable model for our study.

The long non-coding RNA H19 [25], well documented to be involved in cancer progression and metastasis [16], has been shown to be up-regulated under hypoxia conditions. Although it is known that lncRNA H19 contains two different miRNA (miRNA675-3p and miRNA675-5p), their individual role in hypoxia has not been described in literature. As expected, under hypoxic conditions, a ten-fold and five-fold increase in H19 transcription level was detected in both cell models (in U251 and HUVECs, respectively) (**figure 1D, left panel**). Notably, only miRNA675-5p was overexpressed in both cell lines in hypoxic conditions, while no changes were observed for miRNA-675-3p levels (**figure 1D, right panel**).

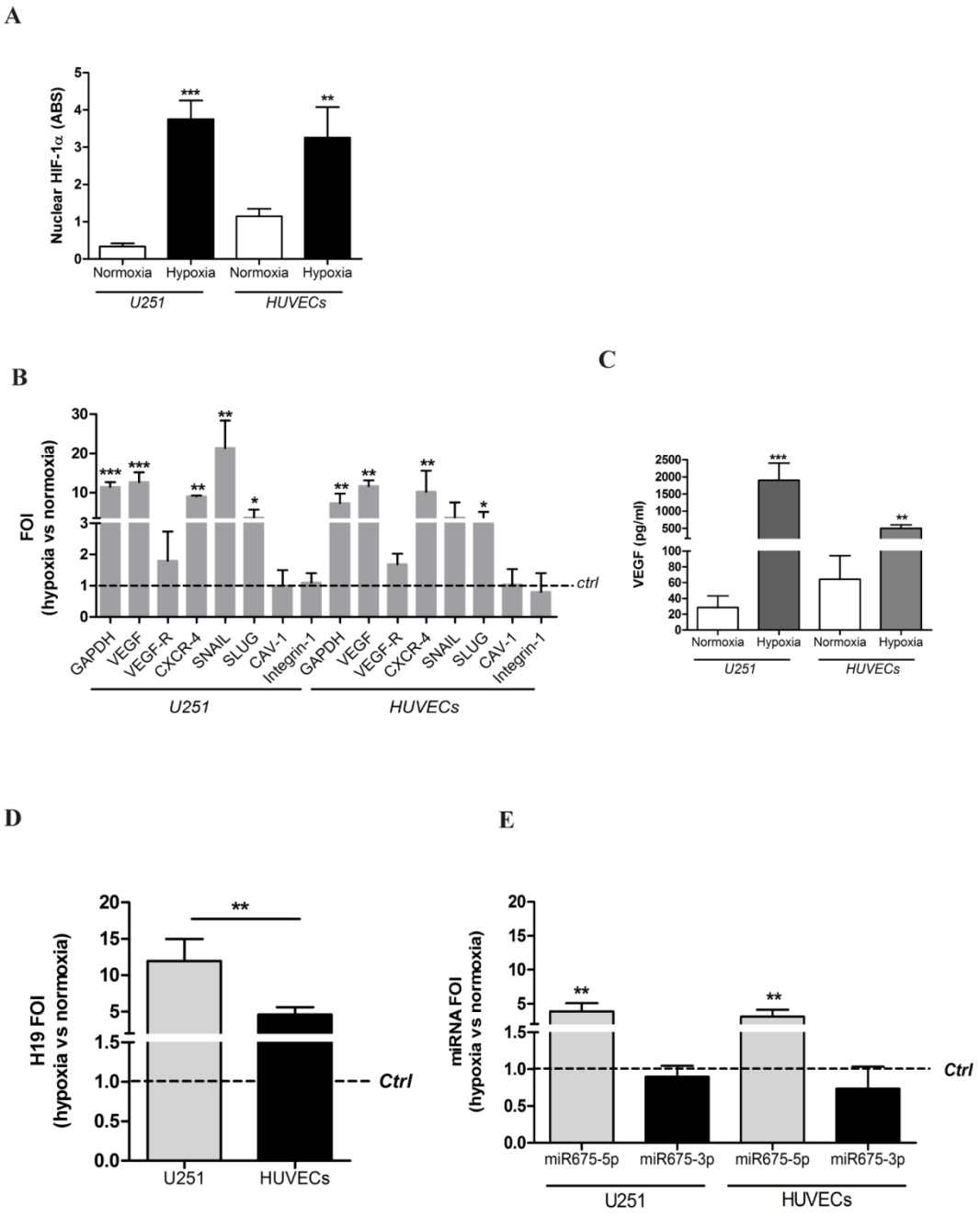

Figure 1: U251 glioma cells and HUVEC endothelial cells as suitable models for hypoxia studies. (A) ELISA assay for HIF-1α performed in U251 and HUVEC nuclear extracts after 6h of hypoxia. Data are expressed as Absorbance (ABS) values at 450nm. **(B)** Real-time PCR performed on U251 and HUVEC cells 6 hours post-hypoxia. Data were normalized for β-actin, and ΔΔct is expressed as fold of induction (FOI) of analyzed genes in hypoxia *vs* normoxia. The dashed line indicates control sample in normoxia. **(C)** ELISA assay for VEGF levels in supernatants from both cell lines after 6 hours of hypoxia. Data are expressed as pg/ml of soluble VEGF. **(D) Left panel:** Real time-PCR for lncRNA H19, after 6h of hypoxia, normalized for β-actin. Data are expressed as FOI of hypoxia-treated cells compared to normoxia samples. **Right panel:** Real time-PCR for H19's microRNAs, miR675-3p and miR675-5p, after 6h of hypoxia. Data were normalized for RNU48. Data are expressed as FOI compared to scramble-treated cells. Values are presented as the mean ± SD. Hypoxia *vs* normoxia * p<0.05; **p<0.01;* **p<0.001.

The presence of the miRNA675-5p is required to induce hypoxia-mediated angiogenesis

With the aim to investigate the role of this microRNA in cell response to hypoxia, we down-regulated miR675-5p levels in hypoxic conditions by transfecting both cell lines with a specific inhibitor. The inhibition of miRNA675-5p in hypoxic conditions correlated with a reduction of HIF-1α activity. Both in endothelial and glioma cell models, miRNA675-5p inhibitor induced a down-regulation of nuclear HIF-1α (**figure 2A and figure S2**), together with a reduction in the expression of its target genes (**figure 2B**). Concerning hypoxia-induced angiogenesis, VEGF mRNA (**figure 2B**) and protein (**figure 2C**) were strongly down-regulated in presence of miRNA inhibitor, both in U251 and HUVEC cells.

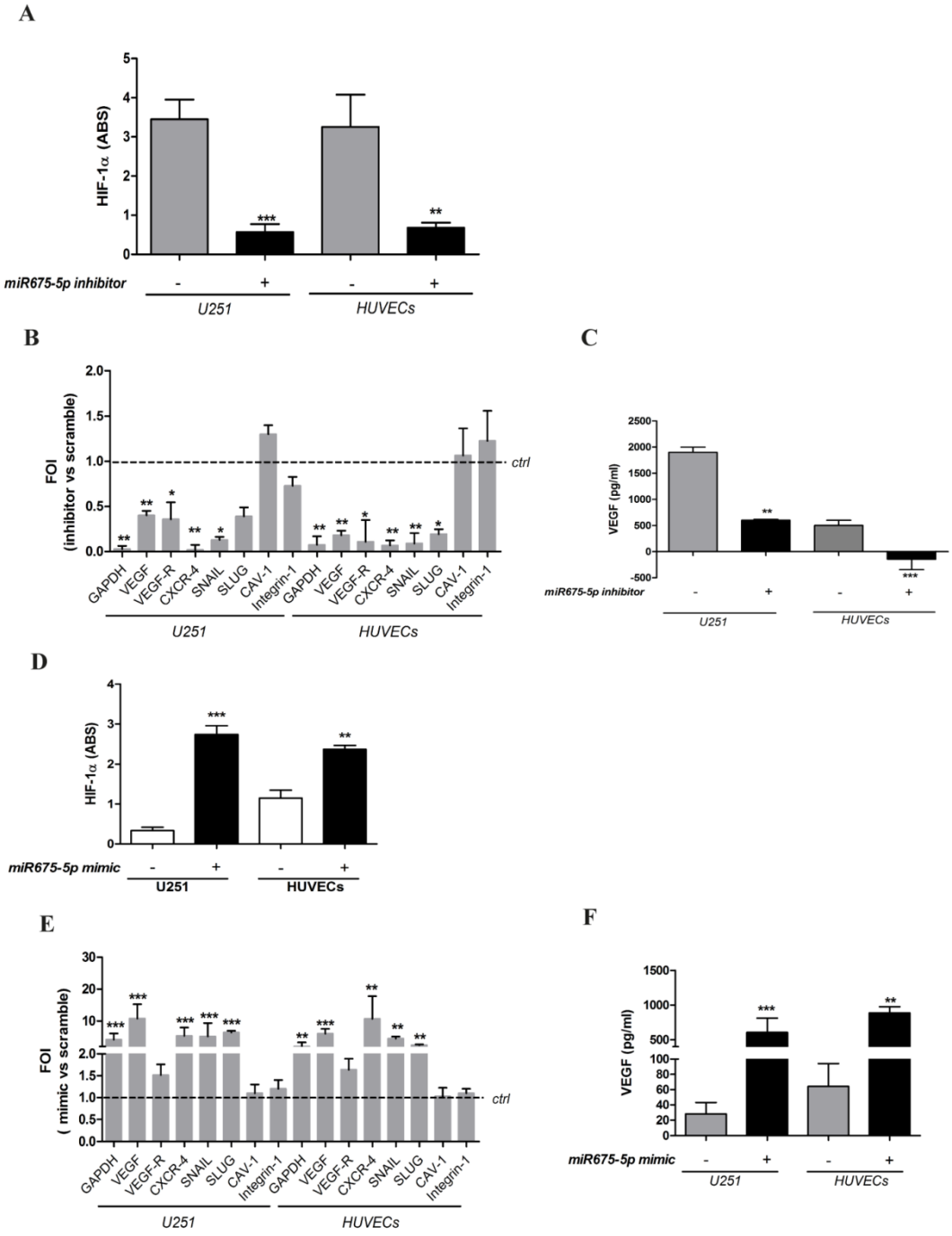

Figure 2: Gain and loss of function suggests a critical role of miR675-5p on hypoxia modulation. (A) ELISA for HIF-1α nuclear level in U251 and HUVECs transfected with miR675-5p inhibitor and exposed to hypoxia for 6h. Data are expressed as ABS values at 450nm. **(B)** Real-time PCR from U251 and HUVECs exposed to hypoxia after miR675-5p inhibitor or scramble control transfection. Data were normalized for β-actin and ΔΔct is expressed as fold of induction (FOI) of indicated genes after inhibitor transfection compared to scramble control (dashed line). **(C)** ELISA assay for VEGF level in supernatant from both cell lines transfected with miRNA inhibitor or negative control and exposed to hypoxia for 6h. Data are expressed as pg/ml of soluble VEGF. Values are presented as the mean ± SD. Inhibitor *vs* scramble * p<0.05; **p<0.0; ***p<0.001. **(D)** HIF-1α nuclear level analyzed by ELISA assay in U251 and HUVEC cells after 18h of miR675-5p mimic transfection in normoxia. Data are expressed as ABS values at 450nm. **(E)** Real-time PCR performed on U251 and HUVEC cells after miR675-5p mimic-transfection. Data were normalized for β-actin, and ΔΔct is expressed as fold of induction (FOI) in cells transfected with mimic compared to control (dashed line). **(F)** ELISA assay for VEGF level in supernatant from both cell lines 18h after mimic transfection. Data are expressed as pg/ml of soluble VEGF. Values are presented as the mean ± SD. Mimic *vs* scramble * p<0.05; **p<0.01;***p<0.001.

No differences were found in cell viability in hypoxia with or without miR675-5p inhibitor (**figure S3**). In order to further investigate the role of miRNA675-5p, cells were also analysed in normoxic conditions overexpressing miRNA675-5p. As shown in **figure 2D and figure S2,** the presence of miRNA675-5p was sufficient to promote a significant HIF-1α nuclear translocation in normoxic conditions. Real time-PCR results confirmed that nuclear HIF-1α induced the transcription of its target genes also in normoxic conditions (**figure 2E**). Similarly, transfection with miRNA675-5p mimic in normoxia

was able to induce, in both cell lines, VEGF secretion as measured by ELISA (**figure 2F**). Tube formation assay in **Figure S4** showed a significant decrease in the number and the length of tubular-like structures when HUVECs were treated in hypoxia with miRNA675-5p inhibitor. Conversely, when HUVECs were treated in normoxia with miRNA675-5p mimic, an increase of tubular-like structures was detected, confirming a functional involvement of this miRNA in the angiogenic process.

MiRNA675-5p drives hypoxic responses in vivo

In order to determine if the presence or depletion of miRNA675-5p causes *in vivo* the same effect observed *in vitro*, a glioma orthotropic murine model was generated by stereotaxic surgery injection of U251-HRE-mCherry cells. In these cells, Luciferase expression controlled by HRE sequences, allows the evaluation of hypoxia levels over time, while the tumour growth can be evaluated by mCherry fluorescence assessment at the same experimental points. Before *in vivo* injection, U251-HRE-mCherry cells were tested *in vitro* (**figure 3A),** and showed an increase of Luciferase activity after transfection with miRNA675-5p mimic compared to control plasmid. The time line in the material and methods section describes the procedure for the *in vivo* treatment. Briefly: starting twelve days post U251-HRE-mCherry cell injection, mice underwent four intravenous administration of miRNA675-5p mimic or scramble as negative control. As previously demonstrated by Lo Dico et al [26] and confirmed in our control mice, eighteen days after glioma cells injection, a strong increase of hypoxia can be detected *in vivo* by using optical imaging techniques (**figure 3B, left panel**). The administration of MiRNA675-5p mimic starting from day 12, before the establishment of hypoxia, anticipated hypoxia induction at day 15 and enforced this as indicated in **figure 3B**. ROI analyses confirmed the results with a statistically significant difference in luciferase emission at day 19 in the mimic-treated group compared to control (**figure 3B, right panel**). Subsequently, both groups were analysed for HIF-1α downstream target and neo-angiogenesis biomarker expression through the use of two different fluorescent probes, targeting CAIX and Integrin α5β3, respectively (**figure 3C, left panel**). HypoxiSense acquisition showed the induction of CAIX expression in mimic-treated mice, in agreement with an increase in HIF-1α activity. At the same time, IntegriSense probe showed an increase in Integrin α5β3 expression correlated to the neo-angiogenesis stimulation. Image quantification confirmed the results observed in fluorescence images (**figure 3C, right panel**).

Finally, tumour growth rate was analysed by evaluation of mCherry signal. Systemically administered miRNA675-5p mimic enhanced tumour growth, as demonstrated by the higher mCherry signal of the treated- group compared to the control group at the end-point (**figure 3D**). This is in agreement with the longitudinal study, where an induction of tumour growth was observed over time in the mimic-treated group (**Figure S5**) and confirmed by the assessment of tumour weight at *ex vivo* examination (**Figure S6**). These data suggest a role for miRNA675-5p in the earlier establishment of the cell response to hypoxia that correlates with the earlier neo-angiogenesis induction and higher tumour growth. To further demonstrate the role of miRNA675-5p in glioblastoma progression, miRNA675-5p inhibitor was administered starting from day 21 post glioma cell injection, when hypoxia was already established, following the scheduling in materials and methods. **Figure 4A (Left panel)** showed that, by abolishing miRNA675-5p levels, HypoxiSense and IntegriSense specific signals were significantly reduced at the end of the treatment. These results were also confirmed by ROI analysis (**figure 4A, right panel).** As regards to tumour growth kinetic, at the end point, we observed a smaller tumour mass in the animal group treated with miRNA675-5p inhibitor compared to the control group and this reduction was already present after the second miRNA675-5p inhibitor administration (**Figure S7**). These results were confirmed by *ex vivo* tumour weight evaluation showing that in inhibitor-treated animals, tumours were characterized by a lower weight (**Figure S6**) compared to tumours from the control groups (both vehicle and scramble groups). *Ex vivo* IHC confirmed the impairing of HIF-1α nuclear translocation after miRNA675-5p inhibitor administration (**Fig.4C**). All *in vivo* data were supported by H&E and IHC analysis (**Figure S8**)

Overall, our data indicate that the inhibition of miRNA675-5p *in vivo* is able *i)* to turn off tumour molecular response to hypoxia *ii)* to constrain angiogenesis and *iii)* to block hypoxia-mediated tumour growth, thus suggesting a therapeutic role for miRNA675-5p inhibitor in glioblastoma.

Study of miRNA675-5p putative target and molecular mechanism

In order to investigate the molecular mechanism driving miRNA675-5p effects, we focused our attention on VHL, a physiological HIF-1α inhibitor, indicated by the miRbase database [27] as putative target for miRNA675-5p. Moreover, it is well known that the loss of VHL, in normoxia, is sufficient not only to stabilize HIF-1α subunits, but also to fully activate HIF-1α-mediated responses [6]. In order to

validate VHL as miRNA target in our experimental model, we transfected U251 cells with different doses of miRNA675-5p mimic. As indicated in **figure 5A,** miRNA transfection induced a dose-dependent reduction in VHL mRNA, while the western blot (**figure 5B)** revealed a reduction in pVHL already occurring after the administration of 5pmoli of miR675-5p mimic. However, luciferase reporter system showed that miR675-5p does not target the VHL gene directly (**figure 5C)** as observed for miR21-5p [28] that has VHL as direct target**.** Overall, our data suggest that miR675-5p is able to affect VHL expression indirectly.

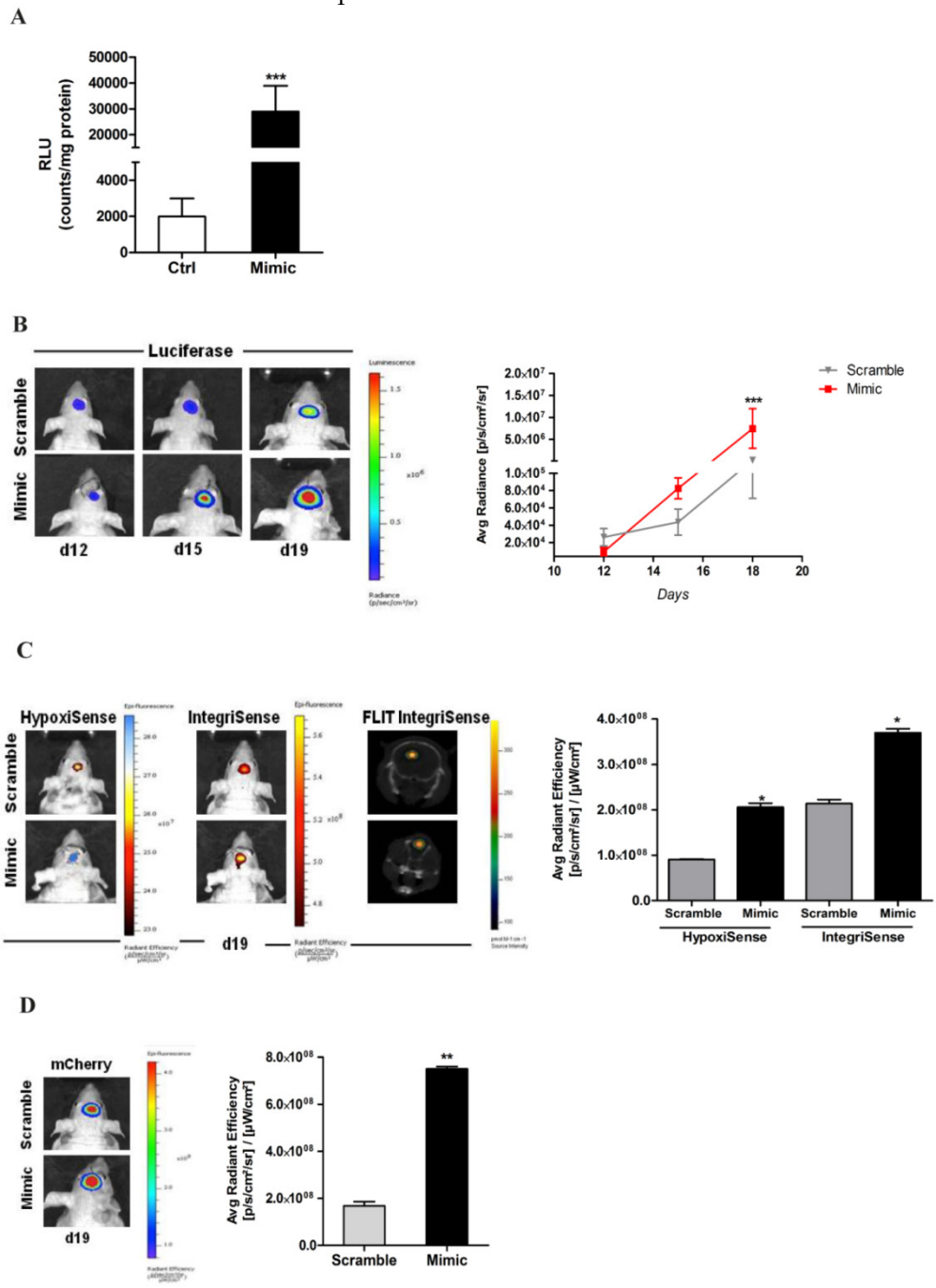

Figure 3: miR675-5p *in vivo* is able to enhance hypoxia establishment and neo-angiogenesis. (A) Luciferase *in vitro* assay performed on U251-HRE lysated cells after 18h of miR675-5p mimic-transfection. Data are represented as RLU (luminescent counts normalized to protein content) of mimic-treated cells compared to scramble-treated cells. Mimic *vs* scramble ***p<0.001. **(B) Left panel:** Representative (n=5) 2D bioluminescent (rainbow scale) of U251-HRE-mCherry tumours in scramble and miR675-5p mimic-treated mice (one of 5 mice) at day 12 (pre-treatment), day 15 (after two doses) and day 19 (end of treatment). Images are presented with the same scale bar**. Right panel:** Graphical representation of Luciferase activity over time during treatment. Data are presented as average radiance (photons/s/cm^2/steradian). **(C) Left panel:** Representative 2D images of mice co-injected with HypoxiSense 680 (BlueHot scale) and IntegriSense 750 (YellowHot scale) and axial images of IntegriSense750 co-registered with CT scan. All scans were performed at the final time point (day 19). **Right panel:** Quantification of HypoxiSense680 and IntegriSense750 fluorescence by ROI analysis for scramble and mimic-treated mice. Data are expressed as average radiance efficiency [(photons/s/cm^2/steradian)/(µW/cm^2)]. **(D) Left panel:** Representative (n=5) 2D mCherry fluorescent signal (rainbow scale) of U251-HRE-mCherry tumours in scramble and miR675-5p mimic-treated mice at day 19. **Right panel:** Graphical representation of mCherry activity at the end of treatment. Data are presented as average radiance efficiency [(photons/s/cm^2/steradian)/(µW/cm^2). Images are presented with the same scale bar. Mimic-treated mice *vs* scramble- treated mice * p<0.05; **p<0.01; ***p<0.001.

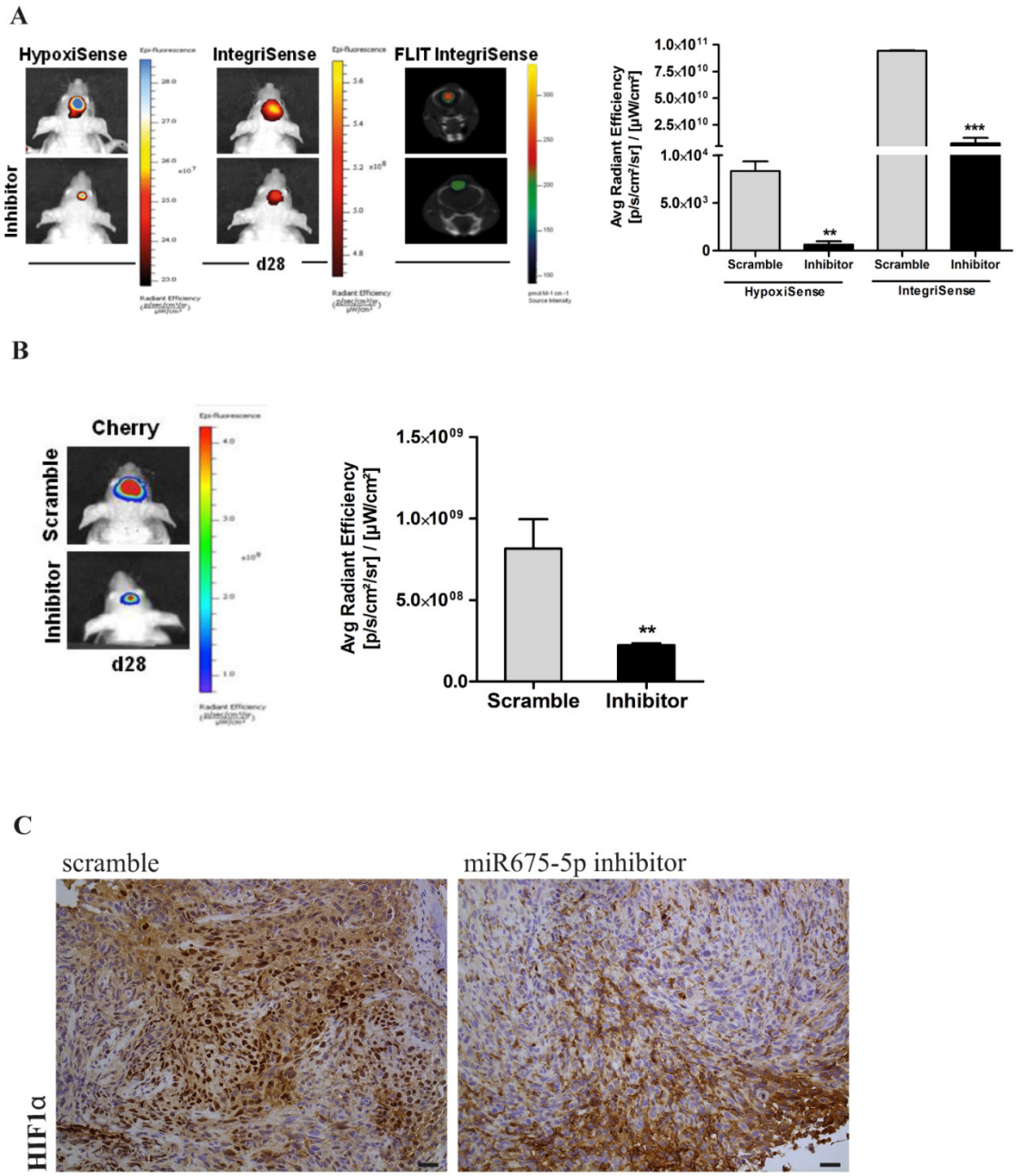

Figure 4: miR675-5p inhibitor counteracts hypoxia-mediated angiogenesis *in vivo*. (A) Left Panel: Representative (n=5) 2D images of scramble or miR675-5p inhibitor-treated mice co-injected with HypoxiSense 680 (BlueHot scale) and IntegriSense 750 (YellowHot scale) and axial images of IntegriSense750 co registered with CT scan. All scans were performed at the final time point (day 28). **Right panel:** Quantification of HypoxiSense 680 and IntegriSense 750 fluorescence by ROI analysis for scramble and miR675-5p inhibitor-treated mice (considering five mice for each treatment). Data are expressed as average radiance efficiency [(photons/s/cm^2/steradian)/(µW/cm^2)]. **(B) Left Panel:** Representative (n=5) 2D mCherry fluorescent signal (rainbow scale) of U251-HRE-mCherry tumours in scramble and inhibitor-treated mice (one of five mouse for each treatment) at day 28. Images are presented with the same scale bar. **Right panel:** Graphical representation of mCherry activity at the end of treatment considering five mice for each treatment. Data are presented as the average radiance efficiency [(photons/s/cm^2/steradian)/(µW/cm^2). Images are presented with the same scale bar. Inhibitor-treated mice *vs* scramble-treated mice * p<0.05; **p<0.01; ***p<0.001. (**C**) Immunoistochemistry for HIF-1α staining in scramble and miR675-inhibitor-treated group (scale bar is represented).

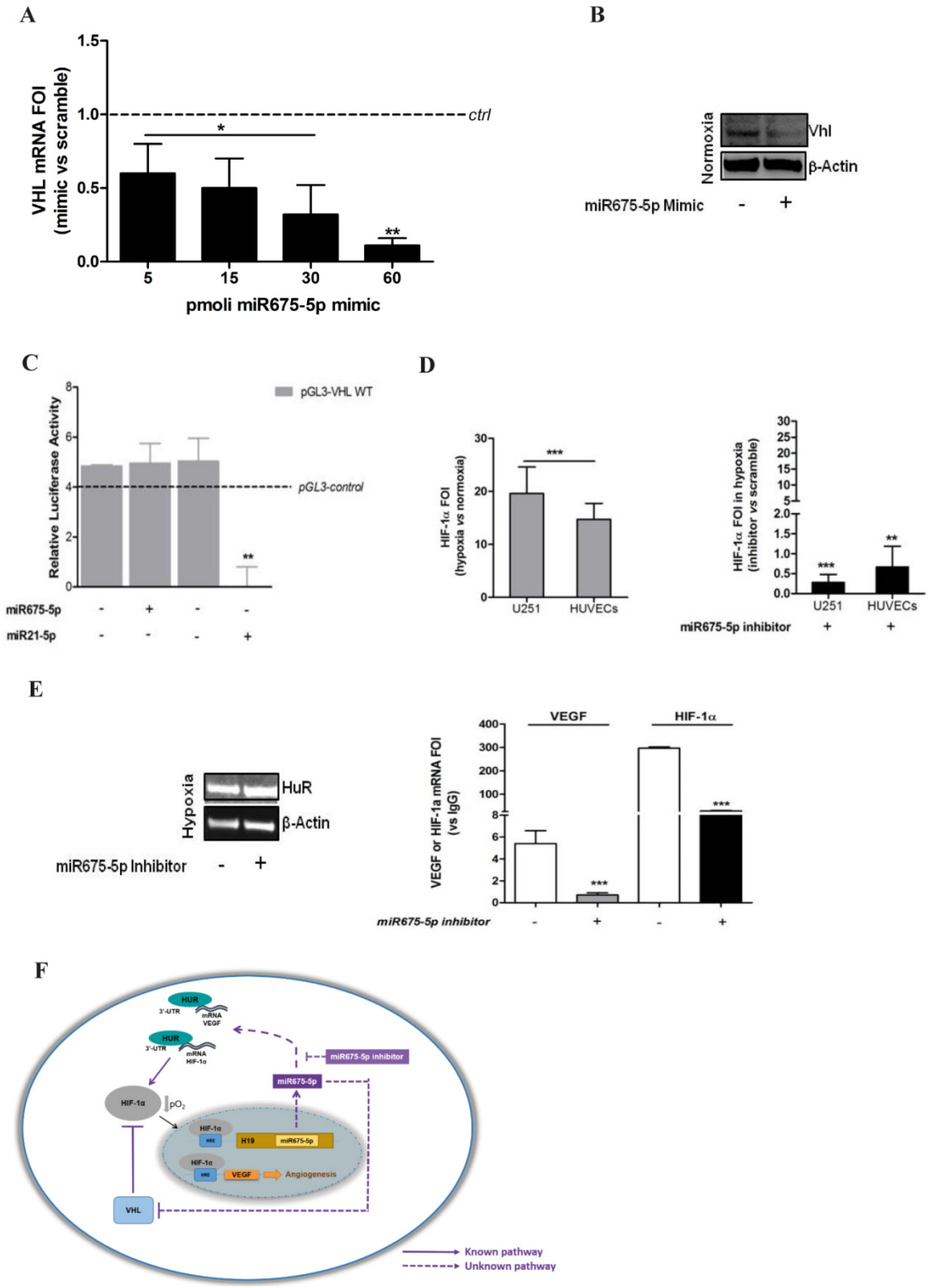

Figure 5: miR675-5p regulates HIF-1α mRNA stability by VHL/HuR axis. (A) Real-time PCR for VHL was done on U251 cells 18h after transfection with 5pM, 15pM, 30pM and 60pM of miR675-5p mimic. The dashed line indicates the control sample (scramble-treated). Values are presented as the mean ± SD. Mimic *vs* scramble * p<0.05; **p<0.01. **(B)** Western Blot for VHL and β-actin from U251 cells transfected with miR675-5p mimic (5pM) or scramble negative control. **(C)** Expression of VHL-regulated miRNA was validated by Luminescence assay kit, a secondary reporter was used for transfection normalization. Data are expressed as Relative Luciferase Activity in pGL3-pVHL-WT construct transfected with miR675-5p or miR21-5p and their relative scrambles. pGL3-control is represented as dashed line. The mean ± SD of three independent experiment is shown, and each sample was assayed in triplicate. **(D) Left panel:** Real-time PCR for HIF-1α performed on U251 and HUVEC cells 6 hours post-hypoxia. Data were normalized for β-actin, and ΔΔCt is expressed as fold of induction (FOI) of HIF-1α in hypoxia *vs* normoxia. **Right panel:** Real-time PCR performed on U251 and HUVEC cells 6 hours post-hypoxia and after miRNA675-5p inhibitor transfection. Data were normalized for β-actin, and ΔΔCt is expressed as fold of induction (FOI) of HIF-1α in hypoxia in inhibitor vs normoxia. **(E) Left panel:** Western Blot for HuR and β-actin from U251 cells transfected with miR675-5p inhibitor (5pM) or scramble negative control after 6h of hypoxia. **Right panel:** RNA-immunoprecipitation for HuR. Real time PCR for VEGF and HIF-1α were performed starting from HuR co-immunoprecipitated RNA in different culture conditions. Ct value was normalized to the Input RNA Ct value. Data are expressed as fold enrichment above the input percentage and presented as the mean ± SD. Inhibitor *vs* scramble negative control ***p<0.001. **(F)** Molecular mechanism of miRNA 675-5p in hypoxia condition. The dashed line indicates our experimental results.

Concerning the down-regulation of nuclear HIF-1α induced by miRNA675-5p depletion in hypoxia, our data demonstrated that neither VHL neither proteasome inhibition were able to rescue nuclear HIF-1α levels **(figure S9**). Therefore, we focused our attention on HIF-1α mRNA. The real time PCR in **figure 5D** indicated that while hypoxia induced an up-regulation of HIF-1α transcript, miRNA675-5p inhibitor treatment strongly inhibited HIF-1α mRNA transcription. These data let us to suppose a transcript destabilization. For this reason, we focused our attention on the RNA binding protein HuR, which has been already demonstrated to stabilize HIF-1α and VEGF mRNAs in low O_2 partial pressure [29, 30]. While no changes in HuR protein levels were detected after miRNA675-5p inhibition in hypoxia (**figure 5E, left panel**), notably, RIP experiments on the amount of HIF-1α and VEGF mRNAs bound to HuR gave an interesting insight. As shown in **figure 5E (right panel)**, levels of HIF-1α and VEGF mRNAs were found significantly decreased when hypoxic U251 cells were treated with miRNA675-5p inhibitor. VEGF and HIF-1α mRNAs were not amplified from the control IgG immunoprecipitation (data not shown).

Discussion

Hypoxia is an essential feature of the neoplastic microenvironment, regulating angiogenesis through multiple pathways, including VEGF signalling [31]. Since the inhibition of angiogenesis in tumorigenesis impairs tumour progression [32], the significance of hypoxia-mediated angiogenesis in driving tumour growth is receiving increased attention. The master gene involved in cell molecular response to hypoxia, HIF-1α, regulates the expression of multiple angiogenic factors. Therefore, targeting HIF-1α for therapy may result in a more comprehensive outcome than the one achieved by any single anti-angiogenic factor [33, 34].

Hypoxia is a predominant feature in glioma and its microenvironment [35], it is associated with tumour growth, progression and resistance to conventional therapy [36]. To better understand the role of hypoxia in glioma establishment and progression, we investigated how U251 glioma cells and an endothelial cell model could react to hypoxic stimuli. Once our experimental models were validated as suitable for hypoxia studies, we investigated tumorigenesis. Recently, we and others have shown that the long non-coding RNA H19 could promote cancer development [16, 17, 37] and Matouk et al have already demonstrated that this oncogenic activity of lncRNA H19 is enhanced under hypoxic stress [16, 25]. Interestingly, recent studies suggest a role of H19 in glioma establishment and progression [38]. Moreover, Shi et al. have showed that H19 and its encoded miRNA675 were positively correlated with glioma grade suggesting a critical role for miRNA675 in tumour malignancy/severity and a possible use as prognostic marker [19]. However, two different miRNA are embedded in H19 and indicated as miR675. Our results showed, for the first time to our knowledge, that hypoxia promotes, together with lncRNA H19, the expression of miRNA675-5p only while no modulation was found for the other miRNA embedded in H19, miRNA 675-3p. MicroRNAs are a new class of master regulators that control gene expression and are responsible for many normal and pathological cellular processes. Several miRNAs, indicated as Hypoxia-Regulated MicroRNAs (HRMs), have already been associated to the hypoxic response. These non-coding RNAs are induced by HIF-1α through direct or indirect activation and cooperate with it by promoting hypoxic response through the down-regulation of normoxic-genes [39]. Interestingly, the vast majority of hypoxia-induced microRNAs are also overexpressed in a variety of human tumours [40]. In literature, the involvement of miR675-5p in tumorigenesis is still controversial, in fact, while it has been indicated as anti-tumoral in small cell lung cancer and prostate cancer [23] [41] it was described as a pro-tumoral molecule in human colorectal and breast cancer [5, 42]. We demonstrated that miR675-5p is a hypoxia-regulated microRNA able, by itself, to mimic a low oxygen condition in normoxia; indeed it was found *i)* essential for hypoxia establishment, *ii)* a stimulator of hypoxia-mediated angiogenesis and *iii)* a promoter of glioma progression. On the other hand, by counteracting tumoral hypoxia-induced events, it may have an important role in therapeutic approaches. In our system, we demonstrated that by abrogating miR675-5p function in hypoxia, HIF-1α activity was completely abolished. This effect reflected also in the down-regulation of hypoxia targets expression and in the negative modulation of angiogenesis, indicating, for the first time, a critical role for miR675-5p in these processes ad suggesting it as a therapeutic agent.

MicroRNAs are pleiotropic modulators, able to regulate simultaneously several target genes and in the case of hypoxia-regulated microRNAs, each HRM is predicted to downregulate more than 10 genes, sometimes as many as 200 [39]. Considering the effects on HIF-1α regulation and the data from miRbase interrogation, among the miR675-5p predicted targets, we focused our attention on pVHL, which targets HIF-1α for proteosomal degradation [43] and whose inhibition in normoxia is sufficient to promote the expression of VEGF [44]. As indicated by

Mack et al. [6], loss of *Vhl* is sufficient to completely dysregulate HIF-1α and to promote its activity. Interestingly, while these authors indicated that VHL deletion did not enhance the growth in subcutaneous tumours derived from primary cells *Vhl*-/-, in our *in vivo* experiments miR675-5p administration and, subsequently, VHL down-modulation, promote tumour growth. This effect could be ascribable to the dual action of the miRNA on glioblastoma cells as well as on endothelial cells that, as indicated by our *in vitro* experiments, respond to miRNA-675 over expression. However, the involvement, in this process of other miR675-5p targets that could reinforce the activity of hypoxia in tumour progression appears conceivable.

When low oxygen induces the expression of HRMs, some genes targeted by these miRNAs stabilize HIF1-α by forming positive-feedback loops: miR-210 could repress glycerol-3-phosphate dehydrogenase 1-like (GPD1L), which, in turn, affects HIF1α stability or miR-424 that, by suppressing cullin2 in human endothelial cells, blocks HIF1α ubiquitination [45].

In our *in vitro* and *in vivo* models the abrogation of miR675-5p expression, although in low oxygen condition, was able to affect both HIF-1α activity and synthesis, thus turning off hypoxic responses, including angiogenesis. The treatment with miR675-5p inhibitor in low oxygen, while did not modulate VHL, eliminated the principal regulator of hypoxia-responsive pathway through the destabilization of HIF-1α mRNA. Taking these results into account, with the hypothesis of the involvement of different partners, and since it has been demonstrated that the RNA binding protein HuR, binds both HIF-1α [29] and VEGF [30] mRNAs increasing their stability, we demonstrated for the first time that the expression of miR675-5p during hypoxia plays a fundamental role in sustaining this mRNA stabilization. Our data, exemplified in **figure 5F,** are in line with recent studies [46, 47] describing the interaction between RNA Binding Proteins and miRNA in post-transcriptional gene regulatory mechanisms. Further studies are required to clarify the interaction between miR675-5p and HuR. In conclusion, in this study we unveiled a key role of miR675-5p in hypoxia where its function is mandatory to support the process, and we identified in miR675-5p a new therapeutic target in tumour progression, where miRNA675-5p inhibition is able to counteract hypoxia process. On the other hand, we demonstrated that miR675-5p could drive angiogenesis, by mimicking hypoxia in a non-hypoxic microenvironment, thus suggesting a novel therapeutic option for angiogenesis promotion.

Materials and Methods

Cell culture and reagents

U251 glioma cells were routinely maintained in RPMI supplemented with 10% heat-inactivated foetal bovine serum, penicillin and streptomycin (50 IU/ml), 2 mM glutamine (Euroclone, UK). HUVECs (C2519A Lonza, Belgium) were grown in endothelial growth medium (EGM, bullet kit, Lonza, Belgium) according to the supplier's instructions. Cells were maintained in a humidified atmosphere of 5 % of CO_2 at 37 °C. During hypoxia experiments, both U251 and HUVEC cells were seeded at 10,000 cells/cm^2 and incubated in a "Hypoxic Chamber" [48] containing 1% O_2 gas mixture for 6 hours (h).

To obtain biochemical VHL inactivation, cells were treated with 100 μM of the hypoxia mimetic agent deferoxamine (DFX, Sigma-Aldrich, St. Louis, MO, USA) for 6 hours before miRNA675-5p inhibitor transfection. DFX was resuspended in distilled sterile water. The proteasome inhibitor MG132 (Calbiochem, San Diego, CA) was dissolved in DMSO solution buffer at 10 mM as a stock solution and cells were treated for 24 hours. DMSO was used as a control vehicle.

Cell transfection

For cell transfection, Attractene Transfection Reagent (cat.number 1051531, Qiagen) was used following the manufacturer's indication. Briefly, U251 and HUVEC cells were seeded at 10,000 cells/cm^2 and transfected with 15pmoles/ml of hsa-mir675-5p inhibitor (cat.number 4464084, Life Technologies, Italy), hsa-mir675-5p mimic (cat.number 4464066, Life Technologies) or scrambled negative control (cat. number 4464058, Life Technologies). Eighteen hours after transfection, the medium was collected and the cells processed for the following assays.

TransAM Kit

An ELISA-based kit (TransAM Kit, Vinci-Biochem, Italy) was used to detect and quantify HIF-1α transcriptional factor activity following the manufacturer's instructions. Briefly, nuclear extracts were firstly prepared using the Nuclear Extract Kit (Vinci-Biochem) and 8μg of the samples were added to the coated plate and analysed at 450nm with Gen5 Microplate Collection & Analysis Software Data (BioTek Instruments, Inc.®). Data were expressed as HIF-1α protein content in the total nuclear extract (Absorbance).

ELISA assay

VEGF concentration was quantified using an ELISA kit (VEGF Human ELISA KitNovex®

cat.number KHG011, Life Technologies) according to the manufacturer's protocol. U251 or HUVEC-conditioned medium was collected after hypoxia treatment or transfection with miR675-5p inhibitor or mimic. Data were expressed as VEGF concentration in pg/ml.

Immunocytochemistry

Immunocytochemistry was performed on PFA 4% fixed cells, and stained with anti-HIF1α 1/100 (HIF-1 alpha Antibody, NB100-105, Novus Biologicals), while the secondary antibody was Alexa-Fluor 488 from Molecular Probes. The nuclei were stained with Hoechst, and preparations were analyzed by confocal microscopy (Nikon A1 Confocal Laser Microscope).

RNA extraction and Real-time PCR

RNA was extracted using the commercially available illustraRNAspin Mini Isolation Kit (GE Healthcare, Italy), according to the manufacturer's instructions. Total RNA was reverse-transcribed to cDNA using the High Capacity cDNA Reverse Transcription Kit (Applied Biosystem, USA). Real-time PCR was performed in duplicates for each data point, and oligonucleotides used are described in **table 1.**

Changes in the target mRNA content relative to an housekeeping gene (β-actin) were determined with the ΔΔct Method. For miRNA expression, 250 ng of RNA were reverse transcripted according to the manufacturer's instructions (cat.number 4366596, TaqManMicroRNA Reverse Transcription, Applied Biosystem). Taqman probes were used to analyse: miR675-5p (cat.number 4440887,Applied Biosystem), miR 675-3p (cat.number 4427975, Applied Biosystem), RNU48 (cat.number 4427975, Applied Biosystem), H19 (Hs00262142_g1 Life Technologies) and Integrin β-1 (HS_00559595, Applied Biosystem). Changes in the target miRNA content relative to housekeeping RNU48 were determined with the ΔΔct Method.

Luminescence Assay Kit

For the study of miR675-5p target, pGL3-control or pGL3-VHL-WT was transfected in U251 cells according to the manufacturer's instructions. After 24h, the medium was changed and the cells were treated for 18h with miR675-5p or miR21-5p and their relative scrambles. At the end of the treatment, the medium was collected and measured for Gaussia Luciferase (GLuc) and the transfection was normalized for the Secreted Alkaline Phosphatase (SEAP). Results were detected by Glomax (GloMax-Multi Detection System; Promega, Madison, WI, USA).).

Endothelial tube formation assay

HUVECs were seeded at 50,000 cells/well and transfection with miRNA mimic, inhibitor or scramble controls. They were then grown in growth factor-reduced Matrigel-coated 24 well plates and incubated up to 2 hours at 37°C (356234,BD Matrigel Matrix). Tube formation was examined under an inverted microscope and photographed at 20× magnification (Leica Microscopy). The length of the cables was measured manually with the IMAGE-J software (http://rsbweb.nih.gov/ij/).

In Vivo Imaging Study Design

Animal experiments were carried out in compliance with the institutional guidelines for the care and use of animals, which have been notified to the Italian Ministry of Health.

U251-HRE human glioma cells (kindly provided by Dr. G. Melillo, National Cancer Institute, Frederick, MD, USA) express the luciferase reporter gene under the control of three copies of an HRE sequence (pGL2-Tk-HRE). This cell line was further stably transfected with pCLL-PGK-mCherry-WPRE lentivirus (kindly provided by Dr. S. Rivella, Weill Cornell Medical College, New York, NY, USA), containing the mCherry gene under the control of the constitutive promoter PGK.

Table 1. Gene primers used to study gene expression profiling.

Gene	Forward primer	Reverse primer
VEGF	CGAGGGCCTGGAGTGTGT	CGCATAATCTGCATGGTGATG
VEGFR1	CGGTCAACAAAGTCGGGAGA	CAGTGCACCACAAAGACACG
H19	GCACCTTGGACATCTGGAGT	TTCTTTCCAGCCCTAGCTCA
HIF-1α	TGATTGCATCTCCATCTCCTACC	GACTCAAAGCGACAGATAACACG
HIF-2	CTTTTCGGGTCTGACAGCCT	TGTGTTCGCAGGAAGCTGAT
CXCR4	TACACCGAGGAAATGGGCTCA	AGATGATGGAGTAGATGGTGGG
VHL 1	GACGGACAGCCTATTTTTGCC	TCCCATCCGTTGATGTGCAA
CAVEOLIN 1	AGACGAGCTGAGCGAGAAGC	CCAGATGTGCAGGAAAGA
SLUG	CATGCCTGTCATACCACAAC	GGTGTCAGATGGAGGAGGG
SNAIL	GCGAGCTGCAGGACTCTAAT	CCCGCAATGGTCCACAAAAC
GAPDH	ATGGGGAAGGTGAAGGTCG	GGGTCATTGATGGCAACAATATC
B-ACTIN	ATCAAGATCATTGCTCCTCCTGA	CTGCTTGCTGATCCACATCTG

Before orthotropic injection, U251-HRE cells were tested for specific miRNA675-5p responsiveness. After 18h of miRNA675-5p mimic or scramble transfection, lysed cells were analyzed on a luminometer (GloMax-Multi Detection System; Promega, Madison, WI, USA). Data were normalized to milligram of proteins measured by Bradford assay and expressed as relative luminescence units (RLU = luciferase counts per milligram proteins). The orthotropic murine model of glioma was obtained, as described by Lo Dico et al [26], by stereotaxic injection of 1×10^5 U251-HRE-mCherry cells in 2 µl of phosphate buffered saline (PBS) into 7- to 8-week-old female nude mice (Harlan Laboratories, USA) at day 0. Following surgery, mice were monitored for recovery until complete awakening.

Animals were grouped as follows:

- Control group (scramble miRNA control, i.v.)
- Mimic-treated group (i.v.)
- Inhibitor-treated group (i.v.)

For all studies, mice were injected every other day for a total of 4 administrations with 1nmole/administration in 100µl of mixture of mimic/inhibitor or scramble. To make the mixture stable, the oligomers were injected by using a kit for delivering miRNA into animal tissue by systemic administration (AteloGene *in vivo* siRNA/miRNA Transfection kit, CosmoBio, DBA, Italy). After mixing miRNA mimic or scramble with Atelogene (1:1), the solution was slowly rotated at 4°C for 20 minutes. Then, samples were centrifuged at 10.000 rpm for 1 minutes at 4°C to eliminate bubbles. For the mimic-study, the i.v. administration was performed between day 12 and day 18 after cell injection; for the inhibitor-study, the treatment was started at day 21 and lasted until day 27.

Optical imaging study design

For the detection of bioluminescence or fluorescence, mice were i.p. anesthetized with Zoletil (40mg/kg, Virbac) and Xilor (8mg/kg, Sigma-Aldrich). The mice were then placed in the light-tight chamber and, 150 mg/kg of luciferin (Beetle Luciferin Potassium Salt, Promega) was intra-peritoneal injected in tumour-bearing mice for bioluminescence imaging (BLI). After biodistribution, bioluminescence was acquired [49]. The mCherry fluorescent signal was also measured by using the appropriate filters (excitation: 590-620 nm; emission=640-660 nm). HypoxiSense680 fluorescent probe (a CAIX-targeted fluorescent *in vivo* imaging agent, PerkinElmer Life Sciences) and IntegriSense750 (targeting αvβ3 integrin, PerkinElmer Life Sciences) were i.v. administered to mice and, after 24h, fluorescence imaging (FLI) was performed, applying the specific filters (excitation: 625-655 nm and emission=690-710 nm; excitation: 695-725 nm and emission=770-790 nm, respectively). All BLI/FLI acquisitions were carried out with IVIS system (PerkinElmer Life Sciences); images were analysed and scaled after completion of all acquisitions, using the Living Image Software. The same region of interest (ROI) was applied on all bioluminescent or fluorescent tumours. Bioluminescence was expressed as average radiance (photons/second/square centimetre/steradian) which is a calibrated measurement of photon emission. Fluorescence was expressed as Average Radiant Efficiency $(p/s/cm^2/sr)/(\mu W/cm^2)$, where the average radiance is further normalized for efficiency of excitation light. Mice were also submitted to 3D diffuse fluorescence imaging tomography (FLIT) for IntegriSense750 probe by supplementing acquisitions with an integrated CT scan.

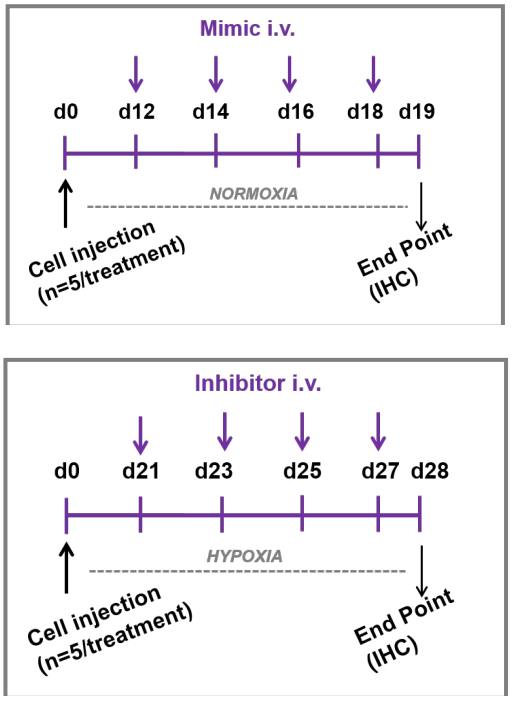

Figure 6. Time lines represent the schedule of i.v. administration for n=5 mice. Upper panel: mir675-5p mimic/scramble administration. Lower panel: miR675-5p inhibitor/scramble administration.

Western Blotting

SDS-PAGE and Western Blotting (WB) were performed according to standard protocols. Briefly, U251 cells after hypoxia treatment or transfection with miR675-5p inhibitor were lysed in lysis buffer containing 15mM Tris/ HCl pH7.5, 120mM NaCl, 25mM KCl, 1mM EDTA, 0.5% Triton X100, Halt Protease Inhibitor Single-Use cocktail (100X,

ThermoScientifc). Whole lysates (15µg per lane) were separated using 4-12% NovexBis-Tris SDS-acrylamide gels (Invitrogen), electro-transferred on Nitrocellulose membranes (Bio-Rad), and immunoblotted with antibodies against the following proteins:, VHL (VHL (FL-181): sc-5575, Santa Cruz Biotechnology, INC.), HuR (HuR (3A2): sc-5261, Santa Cruz Biotechnology, INC.) and β-Actin (Monoclonal anti-β-actin, A5316 Sigma). All secondary antibodies were obtained from Thermo Fisher Scientific. Immunofluorescence was detected using ChemiDoc Biorad acquisition instrument.

RNA immunoprecipitation (RIP)

In order to test the affinity of the RNA binding protein (RBP) HuR for HIF-1α and VEGF mRNAs, a RNA immunoprecipitation was performed, according to the manufacturer's instructions (Imprint RNA Immunoprecipitation Kit, RIP-12RXN, Sigma-Aldrich). After RIP, RNA was identified by RT-PCR. Each RIP Ct value was normalized to the 10% Input RNA fraction Ct value. Data were expressed as fold enrichment above the input percentage.

Immunohistochemistry

At the end of treatment, the animals were sacrificed and their brains were collected, fixed in 10% neutral buffered formalin (Sigma-Aldrich), dehydrated with increasing concentrations of ethanol (75, 85, 95 and 100%, 9 min each), xylene rinsed and finally paraffin-embedded. Longitudinal sections (3–4µm) were cut and stained with Haematoxylin and Eosin (H&E) for morphological evaluation and monoclonal anti-HIF-1α antibody (Novus Biological, CO) and anti-ki67 (Dako, CA, USA) according to the kit manufacturer's instructions.

Statistical analysis

In vitro experiments were repeated three times, giving reproducible results. Data are presented as mean values ± standard deviation (SD) of three independent experiments. For statistical analysis t-test or one- or two-way analysis of variance (ANOVA), followed by Dunnett's or Bonferroni's multiple comparison test, were performed using Prism 4 (GraphPad SoftwareInc., CA, USA).

Supplementary Material

Supplementary figures.
http://www.thno.org/v06p1105s1.pdf

Acknowledgments

This work was supported in part by MIUR Ministero dell'Università e Ricerca Scientifica (FIRB 2012- RBFR12NSCF_002); AIRC Associazione Italiana per la Ricerca sul Cancro (project number 12763) and FP7 funded INSERT project (HEALTH-2012-INNOVATION-1, GA305311). Dr. Diceglie was supported by a fellowship from the Doctorate School of Molecular Medicine, University of Milan, Milan, Italy. The authors wish to thank Dr. G. Melillo, for providing the engineered U251 cells.

Competing Interests

The authors declare no competing interest.

References

1. Vaupel P, Harrison L. Tumor hypoxia: causative factors, compensatory mechanisms, and cellular response. Oncologist. 2004; 9 Suppl 5: 4-9.
2. Folkman J. Angiogenesis in cancer, vascular, rheumatoid and other disease. Nat Med. 1995; 1: 27-31.
3. Mongiardi MP. Angiogenesis and hypoxia in glioblastoma: a focus on cancer stem cells. CNS Neurol Disord Drug Targets. 2012; 11: 878-83.
4. Jensen RL. Hypoxia in the tumorigenesis of gliomas and as a potential target for therapeutic measures. Neurosurg Focus. 2006; 20: E24.
5. Zhong H, De Marzo AM, Laughner E, Lim M, Hilton DA, Zagzag D, et al. Overexpression of hypoxia-inducible factor 1alpha in common human cancers and their metastases. Cancer Res. 1999; 59: 5830-5.
6. Mack FA, Rathmell WK, Arsham AM, Gnarra J, Keith B, Simon MC. Loss of pVHL is sufficient to cause HIF dysregulation in primary cells but does not promote tumor growth. Cancer Cell. 2003; 3: 75-88.
7. Oliver L, Olivier C, Marhuenda FB, Campone M, Vallette FM. Hypoxia and the malignant glioma microenvironment: regulation and implications for therapy. Curr Mol Pharmacol. 2009; 2: 263-84.
8. Brat DJ, Van Meir EG. Vaso-occlusive and prothrombotic mechanisms associated with tumor hypoxia, necrosis, and accelerated growth in glioblastoma. Lab Invest. 2004; 84: 397-405.
9. Ke Q, Costa M. Hypoxia-inducible factor-1 (HIF-1). Mol Pharmacol. 2006; 70: 1469-80.
10. Semenza GL, Nejfelt MK, Chi SM, Antonarakis SE. Hypoxia-inducible nuclear factors bind to an enhancer element located 3' to the human erythropoietin gene. Proc Natl Acad Sci U S A. 1991; 88: 5680-4.
11. Berteaux N, Lottin S, Monte D, Pinte S, Quatannens B, Coll J, et al. H19 mRNA-like noncoding RNA promotes breast cancer cell proliferation through positive control by E2F1. J Biol Chem. 2005; 280: 29625-36.
12. Berteaux N, Aptel N, Cathala G, Genton C, Coll J, Daccache A, et al. A novel H19 antisense RNA overexpressed in breast cancer contributes to paternal IGF2 expression. Mol Cell Biol. 2008; 28: 6731-45.
13. Byun HM, Wong HL, Birnstein EA, Wolff EM, Liang G, Yang AS. Examination of IGF2 and H19 loss of imprinting in bladder cancer. Cancer Res. 2007; 67: 10753-8.
14. Luo M, Li Z, Wang W, Zeng Y, Liu Z, Qiu J. Upregulated H19 contributes to bladder cancer cell proliferation by regulating ID2 expression. FEBS J. 2013; 280: 1709-16.
15. Kim SJ, Park SE, Lee C, Lee SY, Jo JH, Kim JM, et al. Alterations in promoter usage and expression levels of insulin-like growth factor-II and H19 genes in cervical carcinoma exhibiting biallelic expression of IGF-II. Biochim Biophys Acta. 2002; 1586: 307-15.
16. Matouk IJ, DeGroot N, Mezan S, Ayesh S, Abu-lail R, Hochberg A, et al. The H19 non-coding RNA is essential for human tumor growth. PLoS One. 2007; 2: e845.
17. Conigliaro A, Costa V, Lo Dico A, Saieva L, Buccheri S, Dieli F, et al. CD90+ liver cancer cells modulate endothelial cell phenotype through the release of exosomes containing H19 lncRNA. Mol Cancer. 2015; 14: 155.
18. Tsang WP, Ng EK, Ng SS, Jin H, Yu J, Sung JJ, et al. Oncofetal H19-derived miR-675 regulates tumor suppressor RB in human colorectal cancer. Carcinogenesis. 2010; 31: 350-8.
19. Shi Y, Wang Y, Luan W, Wang P, Tao T, Zhang J, et al. Long non-coding RNA H19 promotes glioma cell invasion by deriving miR-675. PLoS One. 2014; 9: e86295.
20. Zhuang M, Gao W, Xu J, Wang P, Shu Y. The long non-coding RNA H19-derived miR-675 modulates human gastric cancer cell proliferation by targeting tumor suppressor RUNX1. Biochem Biophys Res Commun. 2014; 448: 315-22.
21. Li H, Yu B, Li J, Su L, Yan M, Zhu Z, et al. Overexpression of lncRNA H19 enhances carcinogenesis and metastasis of gastric cancer. Oncotarget. 2014; 5: 2318-29.
22. Hernandez JM, Elahi A, Clark CW, Wang J, Humphries LA, Centeno B, et al. miR-675 mediates downregulation of Twist1 and Rb in AFP-secreting hepatocellular carcinoma. Ann Surg Oncol. 2013; 20 Suppl 3: S625-35.

23. Zhu M, Chen Q, Liu X, Sun Q, Zhao X, Deng R, et al. lncRNA H19/miR-675 axis represses prostate cancer metastasis by targeting TGFBI. FEBS J. 2014; 281: 3766-75.
24. Schmitz KJ, Helwig J, Bertram S, Sheu SY, Suttorp AC, Seggewiss J, et al. Differential expression of microRNA-675, microRNA-139-3p and microRNA-335 in benign and malignant adrenocortical tumours. J Clin Pathol. 2011; 64: 529-35.
25. Matouk IJ, Mezan S, Mizrahi A, Ohana P, Abu-Lail R, Fellig Y, et al. The oncofetal H19 RNA connection: hypoxia, p53 and cancer. Biochim Biophys Acta. 2010; 1803: 443-51.
26. Lo Dico A, Valtorta S, Martelli C, Belloli S, Gianelli U, Tosi D, et al. Validation of an engineered cell model for in vitro and in vivo HIF-1alpha evaluation by different imaging modalities. Mol Imaging Biol. 2014; 16: 210-23.
27. Griffiths-Jones S, Grocock RJ, van Dongen S, Bateman A, Enright AJ. miRBase: microRNA sequences, targets and gene nomenclature. Nucleic Acids Res. 2006; 34: D140-4.
28. Zhang KL, Han L, Chen LY, Shi ZD, Yang M, Ren Y, et al. Blockage of a miR-21/EGFR regulatory feedback loop augments anti-EGFR therapy in glioblastomas. Cancer Lett. 2014; 342: 139-49.
29. Galban S, Kuwano Y, Pullmann R, Jr., Martindale JL, Kim HH, Lal A, et al. RNA-binding proteins HuR and PTB promote the translation of hypoxia-inducible factor 1alpha. Mol Cell Biol. 2008; 28: 93-107.
30. Levy NS, Chung S, Furneaux H, Levy AP. Hypoxic stabilization of vascular endothelial growth factor mRNA by the RNA-binding protein HuR. J Biol Chem. 1998; 273: 6417-23.
31. Hockel M, Vaupel P. Tumor hypoxia: definitions and current clinical, biologic, and molecular aspects. J Natl Cancer Inst. 2001; 93: 266-76.
32. Parangi S, O'Reilly M, Christofori G, Holmgren L, Grosfeld J, Folkman J, et al. Antiangiogenic therapy of transgenic mice impairs de novo tumor growth. Proc Natl Acad Sci U S A. 1996; 93: 2002-7.
33. Calvani M, Rapisarda A, Uranchimeg B, Shoemaker RH, Melillo G. Hypoxic induction of an HIF-1alpha-dependent bFGF autocrine loop drives angiogenesis in human endothelial cells. Blood. 2006; 107: 2705-12.
34. Bruick RK, McKnight SL. Building better vasculature. Genes Dev. 2001; 15: 2497-502.
35. Kaur B, Khwaja FW, Severson EA, Matheny SL, Brat DJ, Van Meir EG. Hypoxia and the hypoxia-inducible-factor pathway in glioma growth and angiogenesis. Neuro Oncol. 2005; 7: 134-53.
36. Rankin EB, Giaccia AJ. The role of hypoxia-inducible factors in tumorigenesis. Cell Death Differ. 2008; 15: 678-85.
37. Ayesh S, Matouk I, Schneider T, Ohana P, Laster M, Al-Sharef W, et al. Possible physiological role of H19 RNA. Mol Carcinog. 2002; 35: 63-74.
38. Jiang X, Yan Y, Hu M, Chen X, Wang Y, Dai Y, et al. Increased level of H19 long noncoding RNA promotes invasion, angiogenesis, and stemness of glioblastoma cells. J Neurosurg. 2015: 1-8.
39. Kulshreshtha R, Davuluri RV, Calin GA, Ivan M. A microRNA component of the hypoxic response. Cell Death Differ. 2008; 15: 667-71.
40. Kulshreshtha R, Ferracin M, Wojcik SE, Garzon R, Alder H, Agosto-Perez FJ, et al. A microRNA signature of hypoxia. Mol Cell Biol. 2007; 27: 1859-67.
41. He D, Wang J, Zhang C, Shan B, Deng X, Li B, et al. Down-regulation of miR-675-5p contributes to tumor progression and development by targeting pro-tumorigenic GPR55 in non-small cell lung cancer. Mol Cancer. 2015; 14: 73.
42. Vennin C, Spruyt N, Dahmani F, Julien S, Bertucci F, Finetti P, et al. H19 non coding RNA-derived miR-675 enhances tumorigenesis and metastasis of breast cancer cells by downregulating c-Cbl and Cbl-b. Oncotarget. 2015; 6: 29209-23.
43. Maxwell PH, Wiesener MS, Chang GW, Clifford SC, Vaux EC, Cockman ME, et al. The tumour suppressor protein VHL targets hypoxia-inducible factors for oxygen-dependent proteolysis. Nature. 1999; 399: 271-5.
44. Iliopoulos O, Levy AP, Jiang C, Kaelin WG, Jr., Goldberg MA. Negative regulation of hypoxia-inducible genes by the von Hippel-Lindau protein. Proc Natl Acad Sci U S A. 1996; 93: 10595-9.
45. Shen G, Li X, Jia YF, Piazza GA, Xi Y. Hypoxia-regulated microRNAs in human cancer. Acta Pharmacol Sin. 2013; 34: 336-41.
46. Chang SH, Hla T. Gene regulation by RNA binding proteins and microRNAs in angiogenesis. Trends Mol Med. 2011; 17: 650-8.
47. Ciafre SA, Galardi S. microRNAs and RNA-binding proteins: a complex network of interactions and reciprocal regulations in cancer. RNA Biol. 2013; 10: 935-42.
48. Wu D, Yotnda P. Induction and testing of hypoxia in cell culture. J Vis Exp. 2011.
49. Lo Dico A, Martelli C, Valtorta S, Raccagni I, Diceglie C, Belloli S, et al. Identification of imaging biomarkers for the assessment of tumour response to different treatments in a preclinical glioma model. Eur J Nucl Med Mol Imaging. 2015; 42: 1093-105.